Solvent-aided phase separation in hydrogel towards significantly enhanced mechanoresponsive strength

Haibao Lu,[1]·Ziyu Xing,[1] Mingji Chen,[2] Kai Yu,[3] Yong Qing Fu[4]

[1]National Key Laboratory of Science and Technology on Advanced Composites in Special Environments, Harbin Institute of Technology, Harbin 150080, China

[2]Institute of Advanced Structure Technology, Beijing Institute of Technology, Beijing 100081, China

[3]Department of Mechanical Engineering, University of Colorado Denver, Denver, CO 80217, United States

[4]Faculty of Engineering and Environment, University of Northumbria, Newcastle upon Tyne, NE1 8ST, UK

Haibao Lu, luhb@hit.edu.cn and Kai Yu, KAI.2.YU@UCDENVER.EDU

Abstract: Understanding working principles and thermodynamics behind phase separations, which have significant influences on condensed molecular structures and their performances, can inspire to design and fabricate anomalously and desirably mechanoresponsive hydrogels. However, a combination of techniques from physicochemistry and mechanics has yet been established for the phase separation in hydrogels. In this study, a thermodynamic model is firstly formulated to describe solvent-aided phase and microphase separations in the hydrogels, which present significantly improved mechanoresponsive strengths. Flory-Huggins theory and interfacial energy equation have further been applied to model the thermodynamics of concentration-dependent and temperature-dependent phase separations. An intricately

detailed phase map has finally been formulated to explore the working principle. The thermodynamic methodology of phase separations, combined with the constitutive stress-strain relationships, has a great potential to explore the working mechanisms in mechanoresponsive hydrogels.

Keywords Hydrogel, Mechanoresponsive, Phase separation, Microphase separation

1. Introduction

Phase separation is a classically thermodynamic phenomenon [1-5] in many polymer substances and systems, such as polyelectrolyte complexes [6-7], neurodegeneration [8], proteins [9], DNA [10], liquid-liquid phase separation [11], hydrogels [12-15] and block polymers [16-19]. In a poor solvent, hydrogels often shrink and a distinct interface is formed due to phase separation. By analogy with the coil-to-globule phase transition of polymer solution [12], the molecular phase separations and their transitions are experimentally characterized and investigated using atomic force microscopy [13] and laser scattering confocal microscopy [14]. Whereas the hydrogels are composed of sparse polymer regions, resulting in bicontinuous domains and optical turbidity [13-14].

Solvent-aided phase separation has been applied to the hydrogel, which undergoes concentration-dependent and temperature-dependent shrinking (or deswelling) in solvent. Generally, temperature and concentration of solvent are the two solvent-aided factors to determine the condensed molecular structures of hydrogels, of which the mechanical properties have been significantly improved using phase separations

[12,15]. According to the previous studies [12,15,20], phase separations are divided into phase and microphase types based on the domain sizes of interfaces, whereas the separation process is reversible. Therefore, the techniques of designable and controllable phase separations [21,22] have been applied in the hydrogels for applications such as soft actuators [23], fluidics [24], optics [25], biomedical drug delivery [26] and tissue engineering [27].

Although phase separation plays a key role to design condensed molecule structures and achieve on-demanding properties [1-5], its theoretical understanding and working principle are still challenging issues due to their complexly thermodynamics and interfacial equilibriums at the molecular scales [28]. Furthermore, the working mechanisms of phase separation in the fracture propagation [29] and ultrahigh strain [30-31] have not been fully understood. In this study, Flory-Huggins solution theory, free-energy and interfacial energy equations have been employed and extended to map the solvent-aided phase transitions and separations as well as describe the constitutive stress-strain relationships of hydrogels. Both model strategies of concentration-dependent phase separation and temperature-dependent microphase separation have been proposed to formulate the thermodynamic phase transitions and significantly enhanced mechanoresponsive strengths [32-34]. Finally, the effectiveness of the proposed model is verified by applying it to predict the experimental data of the hydrogels undergoing phase or microphase separation. In comparison with the previous studies [22,32], this paper reports a constitutive model of hydrogels undergoing phase and microphase separations during their swelling.

2. Mapping phase transitions of hydrogel in good and poor solvent

Hydrogel is generally composed of crosslinked gel networks and plenty of water (or solvent) molecules [12,15-16]. In a good solvent (for the interaction parameter ($\chi < 0.5$) of polymer gel and water [1,20]), the gel can be swollen and shows high transparency and elastic property. While it turns to shrink and becomes opaque due to phase separation in poor solvents (e.g., $\chi > 0.5$ [1,20]). When $\chi = 0.5$, the water is named as the θ solvent for polymer gel [1,20]. When a phase separation occurs in a certain environment, due to the chemical bonds or hydrogen bonds between blocks, the average distance between two phases is in tens to hundreds nanometers. Furthermore, microphase separation is a special form of phase separation, where the average distance between two phases is 560 to 880 Å [1,12,15-16].

In good or poor solvents, hydrogel may undergo aggregation structure transition [12,32-34] and phase transition, respectively [12-15,20]. Various phase transitions will lead to different condensed molecule structures [12,15], resulting in a variety of mechanical performances of the hydrogel. Figure 1(a) presents a map of phase states and transitions [32,33] in the hydrogel. The boundary equations of phase transitions can be written as [20,32,33],

$$\text{AB: } \tau = N^{-1/2} \quad \text{EF: } \tau = -N^{-1/2} \tag{1a}$$

$$\text{BG: } \tau = \phi_1 \qquad \text{FH: } \tau = -\phi_1 \tag{1b}$$

$$\text{BD: } \tau = \phi_1^{-\frac{5}{3}} N^{-\frac{4}{3}} \tag{1c}$$

where $\tau = \dfrac{T-\theta}{\theta}$ is the temperature coefficient [20,32,33], T is the temperature, θ is the theta temperature [20], N is the polymerization degree and ϕ_1 is the volume

concentration of gel. Phase transition is generally governed by the Flory-Huggins theory [1,20]. Here the mixing free-energy (ΔF_M) equation is then introduced [1,20],

$$\Delta F_M = N_M k_B T[\frac{\phi_1}{x_1}\ln\phi_1 + \frac{1-\phi_1}{x_2}\ln(1-\phi_1) + \chi\phi_1(1-\phi_1)] \quad (2)$$

where N_M is the monomer number, k_B is the Boltzmann constant, χ is the interaction parameter, x_1 and x_2 represent the number of monomers in the segment of gel and solvent, respectively. Therefore, the phase separation in a good solvent can be obtained based on the equilibrium equation of $\frac{\partial \Delta F_M}{\partial \phi_1} = 0$ [20], $\chi = \frac{\theta}{2T}$ and $\tau = \frac{T-\theta}{\theta}$ [35] as follows,

$$\text{IJ: } \tau = \frac{(2\phi_1 - 1)/2}{\frac{1+\ln\phi_1}{x_1} - \frac{1+\ln(1-\phi_1)}{x_2}} - 1 \quad (3)$$

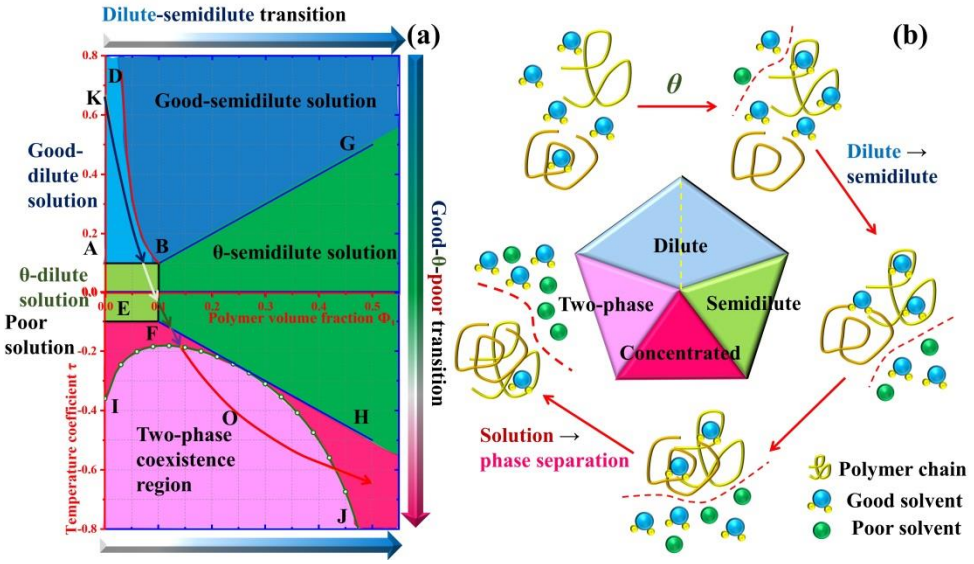

Fig. 1. Schematic illustrations of the hydrogel involved in the phase transition and separation at given constants of $N = 100$, $x_1 = 5$ and $x_2 = 1$. (a) Phase diagrams. (b) Aggregation structure transition and phase separation of hydrogel in poor solvent.

On the other hand, for polyacrylamide (PAAM) hydrogel in the poor

(N,N-dimethylformamide, DMF) solvent [15], the phase transition is originated from the PAAM-water and DMF-water phases. Solvent-aided phase separation is gradually achieved with an increase in the volume concentration of poor DMF solvent in PAAM hydrogel, which undergoes a two-stage phase transition of aggregation structure transition and phase separation, as shown in Fig. 1(b).

Therefore, the phase separation in the poor solvent can be obtained based on the equilibrium equation of $\chi_{pwd} = \phi_{DMF}\chi_{pd} + (1-\phi_{DMF})\chi_{pw}$ [20], $\chi = \frac{\theta}{2T}$ and $\tau = \frac{T-\theta}{\theta}$ [35] as follows,

$$\text{KO: } \tau = \frac{1/2}{\phi_{DMF}\chi_{pd} + (1-\phi_{DMF})\chi_{pw}} - 1 \tag{4}$$

where χ_{pwd} is the interaction parameter of PAAM-water and DMF, ϕ_{DMF} is the volume concentration of DMF in DMF-water phase, χ_{pd} is the interaction parameter of PAAM gel and DMF, χ_{pw} is the interaction parameter of PAAM gel and water.

3. Modelling and experimental verification

As is known, there are many kinds of solvent-aided phase separations owing to the changes in volume concentration or temperature, thus resulting in completely different condensed molecule structures in hydrogels. It is necessary to investigate the thermodynamics of phase transitions and explore the working principles between condensed molecule structures and macroscopic behaviors. Figure 2 plots the phase and microphase separations of PAAM [15] and PNIPAm/PDMA (PNIPAm: poly(*N*-isopropylacrylamide); PDMA: poly(*N*,*N*-dimethylacrylamide)) gels. As reported in Ref. [12], the average distance between PNIPAm and PDMA-water

phases is ranged from 560 to 880 Å, respectively. In the PAAM hydrogel, the poor DMF solvent enables a phase separation between PAAM-water and DMF-water phases, thus resulting in a double network structure in the hydrogel [15]. On the other hand, the PNIPAm/PDMA hydrogel is synthesized from the hydrophilic PDMA, which is covalently grafted onto and chemically crosslinked with PNIPAm (it becomes hydrophobic above 30^{o}C [12]). A microphase separation between PNIPAm and PDMA-water phases occurs with an increase in temperature above 30^{o}C. Due to the differences in molecular structures of phase and microphase separations, the macroscopically optical properties are therefore different from each other.

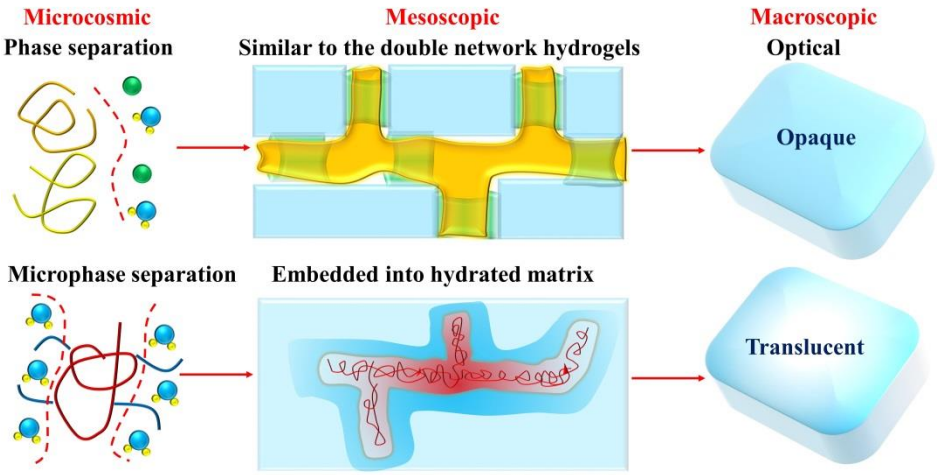

Fig. 2. Schematic illustrations of microcosmic interactions, condensed molecule structures and macroscopically optical properties of the hydrogels undergoing phase and microphase separations, respectively.

3.1 Phase separation of hydrogel in poor solvent

For the phase separation of PAAM hydrogel in the poor DMF solvent, it is governed by the Flory-Huggins theory [37], and elastic free-energy (ΔF_{el}) equation is then used to characterize the thermodynamic behavior,

$$\Delta F_{el} = \frac{1}{2} N_{el} k_B T (\lambda_1^2 + \lambda_2^2 + \lambda_3^2 - 3) \tag{5}$$

where N_{el} is the cross-linking density of elastic network, λ_1, λ_2 and λ_3 represent the stretching ratios of the hydrogels along three directions, respectively. For the homogeneous swelling of isotropic hydrogel, there will be $\lambda_1 = \lambda_2 = \lambda_3 = \lambda$ and $\lambda_1^2 + \lambda_2^2 + \lambda_3^2 = 3\lambda^2 = 3\phi_1^{-2/3}$ [37]. According to chemical potential equilibrium of hydrogel ($\Delta\mu^{pwd} = \frac{\partial \Delta F_M}{\partial n_p} + \frac{\partial \Delta F_{el}}{\partial n_p} = 0$ based on Eqs. (2) and (5), where n_p is the moles of PAAM [1,20]), the dissolution process can be expressed as,

$$\chi_{pwd} = \phi_{DMF}\chi_{pd} + (1-\phi_{DMF})\chi_{pw} = \frac{\ln(1-\phi_{PAAM}) + \phi_{PAAM} + N_{el}\nu\phi_{PAAM}^{1/3}}{-\phi_{PAAM}^2} \tag{6}$$

where ϕ_{DMF} is the volume concentration of DMF in DMF-water phase, ϕ_{PAAM} is the volume concentration of PAAM in PAAM-water phase, N_{el} is the cross-linking density of elastic network and ν is the molar volume ratio of gel monomer to water molecule. Owing to the phase separation, the PAAM-DMF-water ternary system is decomposed into two PAAM-water and DMF-water phases [15]. If the chemical potential of water in these two phases reaches to an equilibrium ($V_{pw}\Delta\mu^{pw} = V_{dw}\Delta\mu^{dw}$ and $\Delta\mu^{dw} = \frac{RTC_0}{N_M}\phi_{DMF} + RTA_2C_0^2\phi_{DMF}^2$), the phase content ($\phi_{pw}$) of PAAM-water is obtained,

$$\phi_{pw} = \frac{V_{pw}}{V_{pw} + V_{dw}} = 1 - \frac{1}{V_{pw}/V_{dw} + 1} = 1 - \frac{1}{\frac{RTC_0}{N_M\Delta\mu^{pw}}\phi_{DMF} + \frac{RTA_2C_0^2}{\Delta\mu^{pw}}\phi_{DMF}^2 + 1} \tag{7}$$

where $\Delta\mu^{pw}$ is the chemical potential of water in PAAM-water phase and it is kept a constant before and after phase separation, $\Delta\mu^{dw}$ is the chemical potential of water

in DMF-water phase and determined by the osmotic pressure [20], V_{pw} and V_{dw} are the volumes of PAAM-water and DMF-water phases, respectively, R is gas constant, C_0 is the concentration coefficient and A_2 is the second virial coefficient [20].

To verify the proposed model and quantitatively separate the effect of phase separation, experimental data [15] of PAAM hydrogel in the poor DMF solvent have been employed to compare with the analytical results obtained using Eq. (6). The analytical results of volume concentration of PAAM as a function of volume concentration of DMF are plotted in Fig. 3. All the parameters used in the Eq. (6) are listed in Table 1.

Table 1. Values of parameters used in Eqs. (6), (7), (8) and (9) for PAAM hydrogel.

χ_{pw}	χ_{pd}	$N_{el}\nu$	$\frac{RTC_0}{N_M \Delta\mu^{pw}}$	$\frac{RTA_2C_0^2}{\Delta\mu^{pw}}$
0.18	0.69	1.0×10^{-3}	28	-21
$N_{el}k_BT$ (MPa)	N_pk_BT (MPa)	ε_{f0}	ε_0	F_s (MJ/m^3)
0.16	700	5.4	23	1.0

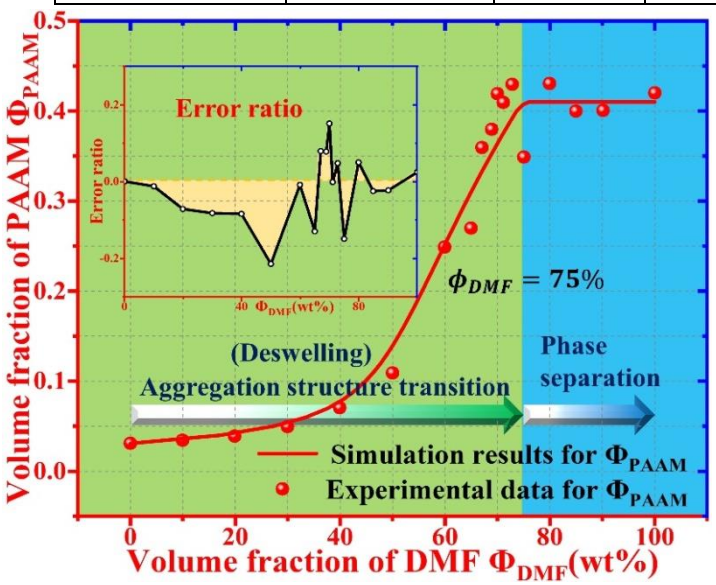

Fig. 3. Comparison of analytical results and experimental data [15] for the PAAM hydrogel, which undergoes two-stage phase transitions of aggregation structure

transition and phase separation in poor DMF solvent.

It is found that the analytical results of the PAAM hydrogel fit well with the experimental data, with an error ratio below ±0.2. The hydrogel undergoes two-stage phase transitions, whereas the first aggregation structure transition [32-33] occurs in the volume concentration of DMF ranged from ϕ_{DMF}=0% to ϕ_{DMF}=75%. During aggregation structure transition, the PAAM hydrogel undergoes a deswelling process because the water molecules are gradually immigrated from hydrogel to DMF, thus resulting in the significant increase in volume concentration of PAAM (ϕ_{PAAM}). With a further increase in ϕ_{DMF} above 75%, the chemically potential equilibrium of water in PAAM-water and DMF-water phases is achieved, resulting in immigration of water and diffusion of DMF forbade. Therefore, the volume concentration of PAAM in hydrogel, which undergoes phase separation in range of ϕ_{DMF}=75% to ϕ_{DMF}=100%, is kept a constant at ϕ_{PAAM}=0.41.

Meanwhile, the PAAM hydrogel obeys the rubber elasticity theory [37], and the modulus (E_{pwd}) and fracture strain (ε_{pwd}) of hydrogel can be expressed as,

$$E_{pwd} = \phi_{PAAM} N_{el} k_B T \tag{8a}$$

$$\varepsilon_{pwd} = \varepsilon_{f0} + \phi_{PAAM} \varepsilon_0 \tag{8b}$$

where ε_{f0} is the initial fracture strain and ε_0 is the fracture strain constant of rubber elasticity network. Therefore, the modulus after phase separation ($E_{pw/dw} = N_{el} k_B T(1-\phi_{pw}) + N_p k_B T \phi_{pw}$, as shown in Fig. S1 and Eq. (S6)) and fracture strain after phase separation ($\varepsilon_{pw/dw}$) can be rewritten, respectively, as,

$$E_{pw/dw}=\frac{N_{el}k_BT}{\frac{RTC_0}{N_M\Delta\mu^{pw}}\phi_{DMF}+\frac{RTA_2C_0^2}{\Delta\mu^{pw}}\phi_{DMF}^2+1}+\frac{(\frac{RTC_0}{N_M\Delta\mu^{pw}}\phi_{DMF}+\frac{RTA_2C_0^2}{\Delta\mu^{pw}}\phi_{DMF}^2)N_pk_BT}{\frac{RTC_0}{N_M\Delta\mu^{pw}}\phi_{DMF}+\frac{RTA_2C_0^2}{\Delta\mu^{pw}}\phi_{DMF}^2+1} \quad (9a)$$

$$F_s=\frac{1}{2}E_{pw/dw}\varepsilon_{pw/dw}^2\Rightarrow\varepsilon_{pw/dw}=\sqrt{\frac{2F_s}{E_{pw/dw}}} \quad (9b)$$

where F_s is the strain energy, N_p is the segment number of PAAM and N_pk_BT is the modulus of PAAM-water phase according to rubber elastic theory [37].

To verify effectiveness of the proposed models, the analytical results of the Young's modulus ($E=E_{pwd}$ and $E_{pw/dw}$) and fracture strain ($\varepsilon_f=\varepsilon_{pwd}$ and $\varepsilon_{pw/dw}$) of the PAAM hydrogels as a function of volume concentration of DMF are plotted and compared with the experimental data [15], as shown in Fig. 4(a). All the parameters used in Eqs. (6), (7), (8) and (9) are listed in Table 1.

Due to the phase transition from aggregation structure transition to phase separation, the Young's modulus (E_{pwd} and $E_{pw/dw}$) of the PAAM hydrogel is significantly increased from $10^{-1.22}$ MPa to $10^{2.57}$ MPa in the volume concentration of DMF ranged from ϕ_{DMF}=70% to ϕ_{DMF}=80%, whereas the fracture strain (ε_f) is sharply decreased from $10^{1.14}$ to $10^{-1.13}$. With an increase in the volume concentration of DMF, the water molecules in PAAM hydrogel are gradually removed, thus resulting in the volume concentration of PAAM gel increased. According to the rubber elasticity theory [37], the mechanical strength of PAAM hydrogel is therefore enhanced and a significantly improved Young's modulus is achieved. However, the fracture strain is decreased due to the increase in the stiffness. On the other hand, the changes in Young's modulus and fracture strain are insignificant, either in aggregation structure transition (0%≤

ϕ_{DMF} ≤70%) or phase separation (80%≤ ϕ_{DMF} ≤100%) state. Figures 4(b) and 4(c) are then plotted to characterize the error ratios of Young's modulus and fracture strain of PAAM hydrogel, respectively. A good agreement of the analytical results and experimental data has been achieved, with the error ratio below to ±0.6. Therefore, the solvent-aided phase transition in PPAM hydrogel has been triggered by the poor DMF solvent, which enables the hydrogel with significantly enhanced Young's modulus and stiffness.

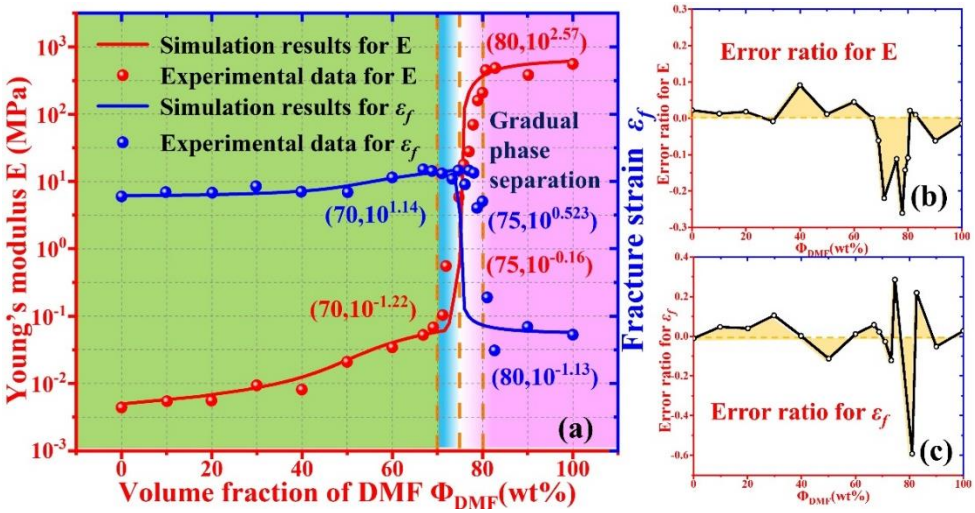

Fig. 4. Comparisons of analytical results and experimental data [15] for the solvent-aided phase transitions in PAAM hydrogel by the poor DMF solvent. (a) For concentration-dependent Young's modulus and fracture strain. (b) Error ratio of Young's modulus. (c) Error ratio of fracture strain.

Furthermore, the constitutive stress-elongation ratio relationship has been investigated for the hydrogel undergoing solvent-aided phase separation by means of poor DMF solvent. According to the extended Maxwell model [38] (as shown in Fig. S1 and Eq. (S10)), the constitutive relationship of stress (σ) as a function of elongation ratio (λ) for the PAAM hydrogel (similar to that of the double network

hydrogel [15]) can be expressed as,

$$\sigma = N_{el}k_BT(\lambda - \frac{1}{\lambda^2}) + \eta\dot{\lambda}[1-\exp(-N_pk_BT\frac{\lambda-1}{\eta\dot{\lambda}})] \quad (10)$$

where η is the viscosity and $\dot{\lambda}$ is the elongation rate.

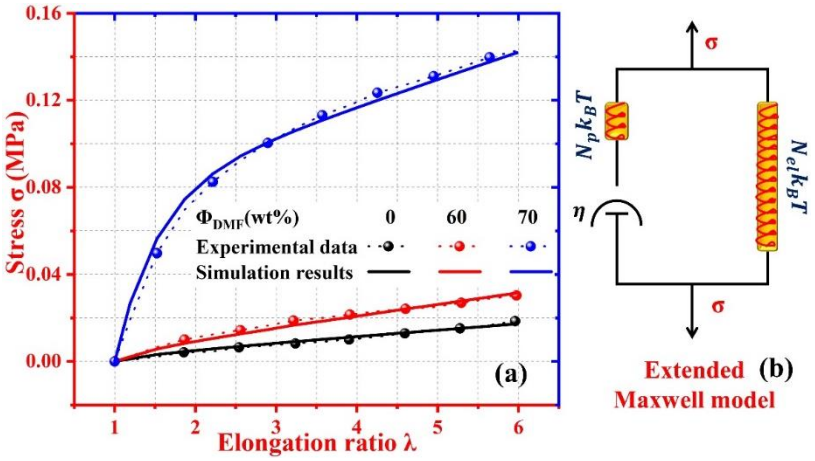

Fig. 5. Comparisons of analytical results and experimental data [15] for the constitutive stress-elongation ratio relationship and concentration-dependent stress strength of PAAM hydrogel, at a given volume concentration of poor DMF solvent at ϕ_{DMF} =0%, ϕ_{DMF} =60% and ϕ_{DMF} =70%.

The analytical results obtained using Eq. (10) are plotted and compared with the experimental data [15] as shown in Fig. 5. A good agreement between the analytical and experimental results has been found as shown in Fig. 5(a). It is revealed that the theoretical model can well describe and predict the relationship between constitutive stress and elongation ratio of the PAAM hydrogels with different volume concentrations of 0%, 60% and 70% poor DMF solvent, where $N_{el}k_BT$ =2.9×10^{-3} MPa, 5.3×10^{-3} MPa and 12.4×10^{-3} MPa, respectively. In the volume concentration of DMF solvent ranged from 0% to 70%, there is no phase separation in the PAAM hydrogel, and the constitutive stress-elongation ratio relationship is governed by the

rubber elasticity theory [37]. With the volume concentration of DMF above 70%, the constitutive relationship of stress-elongation ratio is governed by the extended Maxwell model [38], of which the dual branches are used to characterize the PAAM-water and DMF-water phases, respectively [15], as shown in Fig. 5(b). These experimental and analytical results reveal that the constitutive stress-elongation ratio relationship is critically determined by the phase separation in the PAAM hydrogel. In the phase separation range, even a small increase in elongation ratio can cause a significant increase in the stress. At ϕ_{DMF} =70 wt%, the parameters used in Eq. (10) are $N_{el}k_BT$ =12.4×10^{-3} MPa, η =0.324 MPa·s, $\dot{\lambda} = 0.21s^{-1}$ and N_pk_BT =0.129 MPa. It is revealed that the stress is exponentially increased with respect to the increase in elongation ratio. The experimental results can be well predicted by the proposed models. These analytical and experimental results reveal that the PAAM hydrogel processes a significantly enhanced strength owing to the concentration-dependent phase separation.

3.2 Microphase separation of hydrogel in a good solvent

Due to differently environmental factors and condensed molecule structures, hydrogels will undergo different phase separations and transitions in solvent. As reported in Ref. [12] for the PNIPAm/PDMA hydrogel, the thermo-responsive PNIPAm acts as the main chain and the PDMA works as the side chain. The hydrogel undergoes a classical lower critical solution temperature (LCST) phase transition with an increase in temperature. Above 30^{o}C, the hydrogel undergoes a microphase separation, due to the increased hydrogen bonding strength between hydrophilic

PDMA and water. While the PNIPAm becomes hydrophobic and has a chemical crosslink with PDMA.

According to the interfacial energy equation [16-18,39-42], the free-energy functions of ordered phase (F_{ORD}) and disordered phase (F_{DIS}) are introduced as,

$$F_{ORD} = k_B T(\sqrt{\frac{\chi}{6}}\frac{x_1 l_b}{d/2} + \frac{3}{8}\frac{d^2}{x_1 l_b^2}) \tag{11a}$$

$$F_{DIS} \approx N_{12}\chi k_B T\phi_1(1-\phi_1) \tag{11b}$$

where d is the thickness of interfacial phase, l_b is the segment length, ϕ_1 is the volume content of main chain, $N_{12} = x_1 + x_2$ (x_1 and x_2 are the segment numbers of main chain and side chain, respectively). When the lowest free-energy of ordered phase is achieved (where $\frac{\partial F_{ORD}}{\partial d} = 0$ and $d = l_b N_1^{\frac{2}{3}}\chi^{\frac{1}{6}}$) [16], the free-energy of ordered phase can therefore be obtained as,

$$F_{ORD} \approx 1.2k_B T(x_1\chi)^{\frac{1}{3}} = 1.2k_B T(N_{12}\chi)^{\frac{1}{3}}(\frac{x_1}{N_{12}})^{\frac{1}{3}} = 1.2k_B T(N_{12}\chi)^{\frac{1}{3}}\phi_1^{\frac{1}{3}} \tag{12}$$

Before and after the microphase separation [16-18], the free-energy of the ordered phase is equal to that of the disordered phase, i.e. $F_{ORD} = F_{DIS}$. The temperature coefficient ($\tau = \frac{T-\theta}{\theta}$) [35] can be obtained in combination of Eqs. (11b) and (12),

$$\tau = \frac{1}{2(1.2)^{3/2}} N_{12}\phi_1(1-\phi_1)^{\frac{3}{2}} - 1 \tag{13}$$

During the LCST microphase transition, excessive free-energy (F_{EX}) [35-36] plays an essential role to determine the microphase separation. The equilibrium expression can be then written as [36],

$$\frac{k_B T}{\phi_1 \phi_2} = -\frac{\partial^2 F_{EX}}{\partial \phi_2^2} \tag{14}$$

In combination of Eqs. (11), (12) and (14), the LCST microphase separation can be expressed by,

$$F_{EX} = F_{ORD} \Rightarrow \tau = \frac{1}{2}\left(\frac{0.8}{3}\right)^3 N_{12} \phi_1^{-2} (1-\phi_1)^3 - 1 \tag{15}$$

Here the chemical potential ($\Delta\mu_{DIS}^*$) of hydrogel is obtained by $\frac{\partial(\frac{\partial F_{ORD}}{\partial N_{12}})}{\partial T} = \frac{\partial \Delta\mu_{DIS}^*}{\partial T}$.

The temperature-induced microphase separation ratio (ϕ_T) can be derived as,

$$\phi_T = \left(\frac{3\frac{RC_0}{x_2}\phi_2 + 3RA_2C_0^2\phi_2^2}{0.8k_B}\right)^3 \frac{2N_{12}^2}{\theta}(T - T_C) \tag{16}$$

where T_C =30ºC is the temperature for the microphase separation in the PNIPAm/PDMA hydrogel [12], ϕ_2 is the volume content of side chain of PDMA, and ϕ_T indicates the number of PNIPAm and PDMA components undergoing a microphase separation.

The fracture energy (W_f) is estimated by [1,35-36],

$$W_f = (1-\phi_T)W_{f0} + \phi_T W_{fw} \tag{17}$$

where W_{f0} and W_{fw} are the fracture energies of PNIPAm/PDMA hydrogel and PDMA-water phase, respectively. Equation (17) is derived from Eq. (S6).

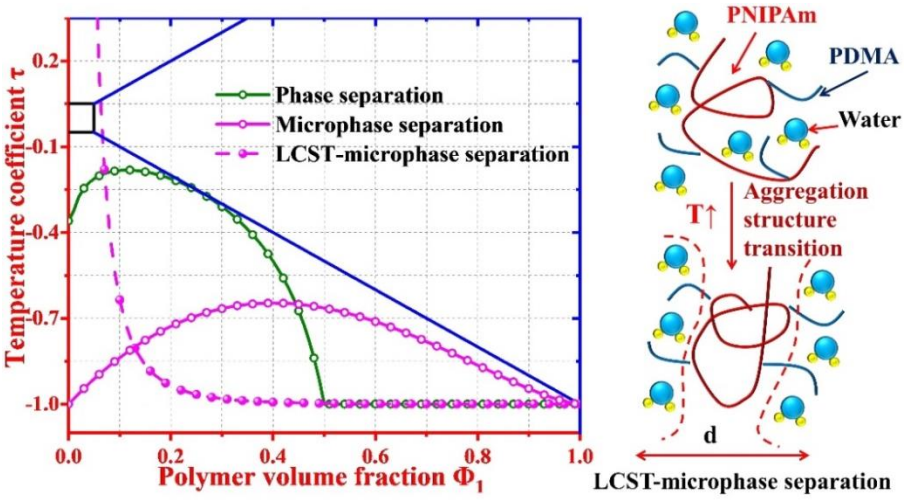

Fig. 6. Schematic diagram of microphase separation and LCST-microphase separation in hydrogel at given constants of $N = 200$, $x_1 = 5$ and $x_2 = 1$.

Figure 6 shows the maps of the phase transitions of aggregation structure transition, phase and LCST microphase separations for the PNIPAm/PDMA hydrogel. According to Ref. [20], both the phase and microphase separations are determined by the same parameter of χN_{12}, and they are χN_{12}=10.5 and χN_{12}=2, respectively.

To verify the accuracy of Eqs. (10) and (17), comparisons of analytical and experimental results [12] of PNIPAm/PDMA hydrogel are shown in Fig. 7, where the experimental results of PNIPAm/PDMA gels were measured in a tensile mode at temperature from 20 to 60°C. Figure 7(a) shows the effect of microphase separation on the mechanical behaviors of hydrogel, of which the continuous and bicontinuous (or chopped) molecule structures are identified as the driving force to determine the mechanical performances. Figure 7(b) plots the analytical and experimental results [12] of fracture energy (W_f) of the PNIPAm/PDMA hydrogel as a function of temperature. The constants used in Eq. (17) are T_C =30°C,

$(\frac{3\frac{RC_0}{x_2}\phi_2 + 3RA_2C_0^2\phi_2^2}{0.8k_B})^3 \frac{2N_{12}^2}{\theta}$ =0.01K^{-1}, W_{f0} =40 J/m^2 and W_{fw} =3110 J/m^2. It is revealed that the fracture energy is increased with an increase in temperature, revealing a positive temperature coefficient (PTC). Above T_C =30ºC, the hydrogel undergoes an LCST microphase separation for PNIPAm and PDMA-water phases, whereas the main chain of PNIPAm turns to be hydrophobic [12]. With a further increase in temperature, the microphase separation enable continuous PNIPAm-PDMA-water formed due to the increased bonding strength between PDMA and water, thus resulting in the fracture energy increased.

On the other hand, the effect of microphase separation on the constitutive stress-elongation ratio relationship is further investigated to explore the working principle of significantly improved mechanical strength in PNIPAm/PDMA hydrogel. As shown in Fig. 7(c), analytical and experimental results [12] of stress with respect to elongation ratio of PNIPAm/PDMA hydrogels have been plotted and compared, at given temperatures of 20ºC, 35ºC, 40ºC, 50ºC and 60ºC. The values of parameters used in Eq. (10) are collected in Table 2, at a given $\dot{\lambda} = 0.06s^{-1}$.

Table 2. Values of parameters used in Eq. (10) for PNIPAm/PDMA hydrogel.

T(ºC)	$N_{el}k_BT$ (kPa)	η (kPa·s)	N_pk_BT (kPa)
20	1.80	/	/
35	2.88	50.0	9.0
40	4.86	80.0	14.4
50	5.61	83.3	15.3
60	6.66	143.3	25.8

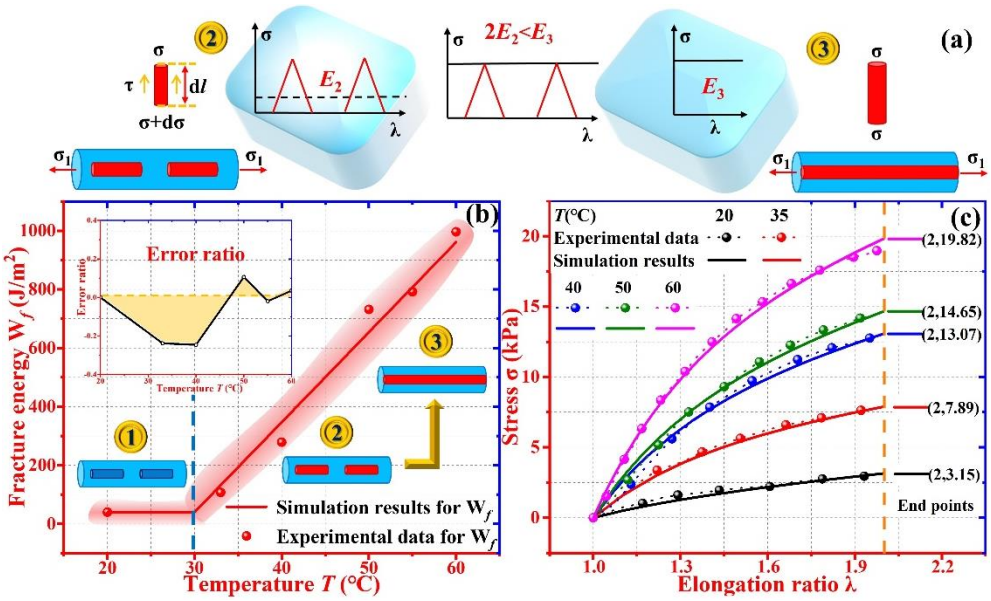

Fig. 7. Comparisons of analytical results and experimental data [12] for the PNIPAm/PDMA hydrogel. (a) Working principle of microphase separation on mechanical property of hydrogel. (b) For temperature-dependent fracture energy. (c) For constitutive stress-elongation ratio relationship and stress strength at various temperatures of 20°C, 35°C, 40°C, 50°C and 60°C.

With an increase in temperature, the stress is gradually increased from 3.15 kPa to 19.82 kPa (with the increment of 529.2%) at the same elongation ratio of λ=2.0. Above T_C=30°C, the stress of PNIPAm/PDMA hydrogel is significantly increased from 7.89 kPa, 13.07 kPa, 14.65 kPa to 19.82 kPa at the temperatures of 35°C, 40°C, 50°C and 60°C due to the microphase separation. With a further increase in temperature, the microphase separation is therefore increased, due to the enhanced bonding strength between PNIPAm and PDMA-water phases. Therefore, the temperature-dependent fracture energy is clearly observed. That is to say, the working principle of temperature-dependent microphase separation is to enable the PNIPAm/PDMA gel and water continuously connected to resist to externally

mechanical loading.

Finally, the effect of microphase separation on crack bifurcation of PNIPAm/PDMA hydrogel has been investigated using the extended Maxwell model [38]. Before and after crack bifurcations, the constitutive stress-elongation ratio relationships can be expressed as,

$$\sigma = N_{el}k_BT(\lambda - \frac{1}{\lambda^2}) + \eta\dot{\lambda}[1-\exp(-N_pk_BT\frac{\lambda-1}{\eta\dot{\lambda}})] \quad (18a)$$

$$\sigma = K\{N_{el}k_BT(\lambda - \frac{1}{\lambda^2}) + \eta\dot{\lambda}[1-\exp(-N_pk_BT\frac{\lambda-1}{\eta\dot{\lambda}})]\} \quad (18b)$$

where K is stress reduction coefficient of the crack bifurcation.

Figure 8 plots the analytical and experimental results [12] of the stress with respect to elongation ratio for the PNIPAm/PDMA hydrogel undergoing temperature-dependent microphase separation. Values of the parameters used in Eq. (18) have been presented in Table 3, at $\dot{\lambda} = 0.06s^{-1}$. A good agreement between the analytical and experimental results has been found. With an increase in temperature from 40ºC, 50ºC to 60ºC, the crack bifurcation stresses (σ) are significantly increased from 13.98 kPa, 19.07 kPa to 23.02 kPa. Whereas the crack bifurcation strains (λ) are increased from 2.27 (227%), 3.11 (311%) to 3.83 (383%). It is expected that the improved crack bifurcation is resulted from the microphase separation. With an increase in temperature, the microphase separation is beneficial to enhance the bonding strength between PNIPAm/PDMA with water, thus resulting in the enhanced PNIPAm-PDMA-water bonding and crack bifurcation strength. Therefore, the PNIPAm/PDMA hydrogel reveals a significantly improved crack

bifurcation strength due to the temperature-dependent microphase separation. Finally, the divergences between the analytical and experimental results are calculated by the correlation index (R^2), which are 98.08%, 98.01% and 98.79% at 40°C, 50°C and 60°C, respectively.

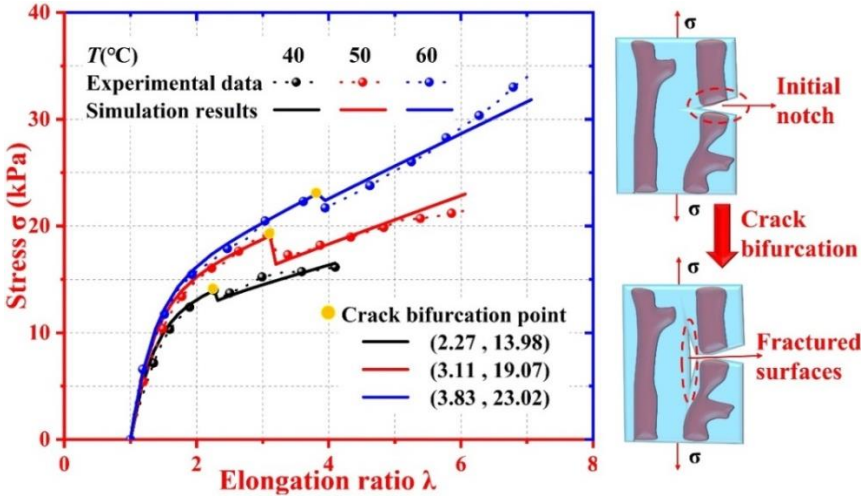

Fig. 8. Comparisons of analytical results and experimental data [12] for the temperature-dependent crack bifurcation strength in PNIPAm/PDMA hydrogel.

Table 3. Values of parameters used in Eq. (18) for PNIPAm/PDMA hydrogel.

T(°C)	$N_{el}k_BT$ (kPa)	η (kPa·s)	N_pk_BT (kPa)	K
40	1.89	171.7	30.9	0.922
50	2.62	186.7	33.6	0.850
60	3.12	188.3	33.9	0.957

4. Conclusion

In this study, we propose a thermodynamic model strategy to study the significantly improved mechanoresponsive strengths in the hydrogel, which undergoes a phase separation in a poor solvent or a microphase separation in a good solvent. The phase and microphase separations have been identified as the driving forces to determine the mechanical properties, by means of continuously and bicontinuously condensed molecule structures. The working principles of significantly improved Young's modulus, stress strength, fracture energy and crack bifurcation strength have been

explored and discussed by the proposed models. It is demonstrated that the theoretical framework can provide an effective approach to characterize and predict the mechanical behavior of hydrogels. Finally, the analytical results have been well verified by the experimental ones reported in literature. This study is expected to provide a fundamental model strategy to formulate the thermodynamic phase and microphase separations in the hydrogels with significantly improved mechanical behaviors.

Acknowledgements

This work was financially supported by the National Natural Science Foundation of China (NSFC) under Grant No. 11725208 and Newton Mobility Grant (IE161019) through Royal Society and NFSC.

References

[1] Flory, P.J.: Principles of polymer chemistry. Cornell University Press, New York (1953)

[2] Flory, P.J.: Molecular size distribution in three dimensional polymers. I. Gelation. J. Am. Chem. Soc. **63,** 3083-3090 (1941)

[3] Flory, P.J.: Thermodynamics of high polymer solutions. J. Chem. Phys. **10,** 51-61 (1942)

[4] Flory, P.J.: Constitution of three-dimensional polymers and the theory of gelation. J. Chem. Phys. **46**, 132-140 (1942)

[5] Flory, P.J.: Introductory lecture faraday discussions of the chemical society. **57,** 7-18 (1974)

[6] Van der Gucht, J., Spruijt, E., Lemmers, M., et al.: Polyelectrolyte complexes: Bulk phases and colloidal systems. J. Colloid Interf. Sci. **361,** 407-422 (2011)

[7] Murakawa, K., King, D.R., Sun, T., et al.: Polyelectrolyte complexation via viscoelastic phase separation results in tough and self-recovering porous hydrogels. J. Mater. Chem. B **7,** 5296-5305 (2019)

[8] Shana, E.G.: Matter over mind: Liquid phase separation and neurodegeneration. J. Biol. Chem. **294,** 7160-7168 (2019)

[9] Harmon, T.S., Holehouse, A.S., Rosen, M.K., et al.: Intrinsically disordered linkers determine the interplay between phase separation and gelation in multivalent proteins Elife **6,** e30294 (2017)

[10] McSwiggen, D.T., Hansen, A.S., Teves, S.S., et al.: Evidence for DNA-mediated nuclear compartmentalization distinct from phase separation. Elife **8,** e47098 (2019)

[11] Meszaros, B., Erdos, G., Szabo, B., et al.: PhaSePro: the database of proteins driving liquid-liquid phase separation. Nucleic Acids Res. **48,** D360-D367 (2020)

[12] Guo, H., Sanson, N., Hourdet, D., et al.: Thermoresponsive toughening with crack bifurcation in phase-separated hydrogels under isochoric conditions Adv. Mater. **28,** 5857–5864 (2016)

[13] Tian, F.L., Wang, H., Li, H.W., et al.: Molecular simulation of diffusion of rigidity-tuned nanoparticles in biological hydrogels. Acta. Mech. Sinica. **35,** 376-383 (2019)

[14] Wang, M., Liu, S.B., Li, F.: Imaging oxygen microenvironment in hydrogel microwell array. Acta. Mech. Sinica. **35,** 321-328 (2019)

[15] Sato, K., Nakajima, T., Hisamatsu, T., Nonoyama, T., et al.: Phase-separation-induced anomalous stiffening, toughening, and self-healing of polyacrylamide gels. Adv. Mater. **27,** 6990–6998 (2015)

[16] Hadjichristidis, N., Pispas, S., Floudas, G.: Block copolymers: synthetic strategies, physical properties, and applications. John Wiley & Sons, Inc., Canada: (2003)

[17] Rumyantsev, A.M., de Pablo, J.J.: Microphase separation in polyelectrolyte blends: weak segregation theory and relation to nuclear “pasta”. Macromolecules **53,** 1281-1292 (2020)

[18] Bates, C.M., Bates, F.S.: 50th Anniversary perspective: block polymers-pure potential. Macromolecules **50,** 3-22 (2017)

[19] Groot, R.D., Madden, T.J.: Dynamic simulation of diblock copolymer microphase separation. J. Chem. Phys. **108,** 8713-8724 (1998)

[20] Gennes, P.G.: Scaling concepts in polymer physics. Cornell University Press, Ithaca and London (1979)

[21] Yoshida, R., Uchida, K., Kaneko, Y., et al.: Comb-type grafted hydrogels with rapid deswelling response to temperature changes. Nature **374,** 240-242 (1995)

[22] Li, M., Zhang, H.X., Zhao, Z.L., et al.: Surface effects on cylindrical indentation of a soft layer on a rigid substrate. Acta Mech.Sin. **36,** 422-429 (2020)

[23] Namdar, A.H., Mazaheri, H. Kinetics of swelling of cylindrical temperature-responsive hydrogel: a semi-analytical study. Int. J. Appl. Mech. **12,** 2050090 (2020)

[24] Beebe, D.J., Moore, J.S., Bauer, J.M., et al.: Functional hydrogel structures for autonomous flow control inside microfluidic channels. Nature **404,** 588-590 (2000)

[25] Dong, L., Agarwal, A.K., Beebe, D.J., et al.: Adaptive liquid microlenses activated by stimuli-responsive hydrogels. Nature **442,** 551-554 (2006)

[26] Coughlan, D.C., Quilty, F.P., Corrigan, O.I.: Effect of drug physicochemical properties on swelling/deswelling kinetics and pulsatile drug release from thermoresponsive poly(N-isopropylacrylamide) hydrogels. J. Control. Release **98,** 97-114 (2004)

[27] Klouda, L., Mikos, A.G.: Thermoresponsive hydrogels in biomedical applications. Eur. J. Pharm. Biopharm. **68,** 34-45 (2008)

[28] Halperin, A., Kröger, M., Winnik, F.M.: Poly(N-isopropylacrylamide) phase diagrams: fifty years of research. Angew. Chem., Int. Ed. **54,** 15342-15367 (2015)

[29] Gong, J.P., Katsuyama, Y., Kurokawa, T., et al.: Double-network hydrogels with extremely high mechanical strength. Adv. Mater. **15,** 1155-1158 (2003)

[30] Kamata, H., Akagi, Y., Kayasuga-Kariya, Y., et al.: “Nonswellable” hydrogel without mechanical hysteresis. Science **343,** 873-875 (2014)

[31] Xia, L.W., Xie, R., Ju, X.J., et al.: Nano-structured smart hydrogels with rapid response and high elasticity. Nat. Commun. **4,** 2226 (2013)

[32] Wu, Y., Hao, X.P., Xiao, R., et al.: Controllable bending of bi-hydrogel strips with differential swelling. Acta Mech. Solida Sin. **32,** 652-662 (2019)

[33] Zhong, D.M., Xiang, Y.H., Liu, J.J., et al.: A constitutive model for multi network elastomers pre-stretched by swelling. Extreme Mech. Lett. **40,** 100926 (2020)

[34] Huang, R., Zheng, S.J., Liu Z.S., et al.: Recent advances of the constitutive models of smart materials- hydrogels and shape memory polymers. Int. J. Appl. Mech. **12,** 2050014 (2020)

[35] Hamada, F., Fujisawa, K., Nakajima, A.: Lower critical solution temperature in linear polyethylene-n-alkane systems. Polym. J. **4,** 316-322 (1973)

[36] Taylor, L.D., Cerankowski, L.D.: Preparation of films exhibiting a balanced temperature dependence to permeation by aqueous solutions-a study of lower consolute behaviour. J. Polym. Sci. Pol. Chem. **13,** 2551-2570 (1975)

[37] Treloar, L.R.G.: The physics of rubber elasticity. Oxford University, New York (1975)

[38] Lu. H.B., Xing, Z.Y., Hossain, M., et al.: Modeling strategy for dynamic-modal mechanophore in double-network hydrogel composites with self-growing and tailorable mechanical strength. Compos. Part B-Eng. **179,** 107528 (2019)

[39] Helfand, E. Tagami, Y.: Theory of the interface between immiscible polymers. Polym. Lett. **9,** 741-746 (1971)

[40] Xiao, R., Qian, J., Qu, S.X.: Modeling gel swelling in binary solvents: a thermodynamic approach to explaining cosolvency and cononsolvency effects. Int. J. Appl. Mech. **11,** 1950050 (2019)

[41] Bishay, P.L., Sladek, J., Fabry, N., et al.: Perturbation finite element solution for chemo-elastic boundary value problems under chemical equilibrium. Acta Mech. Sin. **35,** 981-991 (2019)

[42] Bruhn, O.T.: From basic relations to finite deformation From basic relations to finite deformation. Acta Mech. Sin. **36,** 472-492 (2020)

Table caption

Table 1. Values of parameters used in Eqs. (6), (7), (8) and (9) for PAAM hydrogel.

Table 2. Values of parameters used in Eq. (10) for PNIPAm/PDMA hydrogel.

Table 3. Values of parameters used in Eq. (18) for PNIPAm/PDMA hydrogel.

Figure caption

Fig. 1. Schematic illustrations of the hydrogel involved in the phase transition and separation at given constants of $N = 100$, $x_1 = 5$ and $x_2 = 1$. (a) Phase diagrams. (b) Aggregation structure transition and phase separation of hydrogel in poor solvent.

Fig. 2. Schematic illustrations of microcosmic interactions, condensed molecule structures and macroscopically optical properties of the hydrogels undergoing phase and microphase separations, respectively.

Fig. 3. Comparison of analytical results and experimental data [15] for the PAAM hydrogel, which undergoes two-stage phase transitions of aggregation structure transition and phase separation in poor DMF solvent.

Fig. 4. Comparisons of analytical results and experimental data [15] for the

solvent-aided phase transitions in PAAM hydrogel by the poor DMF solvent. (a) For concentration-dependent Young's modulus and fracture strain. (b) Error ratio of Young's modulus. (c) Error ratio of fracture strain.

Fig. 5. Comparisons of analytical results and experimental data [15] for the constitutive stress-elongation ratio relationship and concentration-dependent stress strength of PAAM hydrogel, at a given volume concentration of poor DMF solvent at ϕ_{DMF} =0%, ϕ_{DMF} =60% and ϕ_{DMF} =70%.

Fig. 6. Schematic diagram of microphase separation and LCST-microphase separation in hydrogel at given constants of $N = 200$, $x_1 = 5$ and $x_2 = 1$.

Fig. 7. Comparisons of analytical results and experimental data [12] for the PNIPAm/PDMA hydrogel. (a) Working principle of microphase separation on mechanical property of hydrogel. (b) For temperature-dependent fracture energy. (c) For constitutive stress-elongation ratio relationship and stress strength at various temperatures of 20°C, 35°C, 40°C, 50°C and 60°C.

Fig. 8. Comparisons of analytical results and experimental data [12] for the temperature-dependent crack bifurcation strength in PNIPAm/PDMA hydrogel.